DOI: 10.1021/ma1011842

Macromolecules
ARTICLE

Step-Cycle Mechanical Processing of Gels of sPP-*b*-EPR-*b*-sPP Triblock Copolymer in Mineral Oil

Zhigang Wang,[†,⊥,#] Yanhua Niu,[⊥] Glenn H. Fredrickson,[†] Edward J. Kramer,*[,†] Yong-Woo Shin,[‡] Fumihiko Shimizu,[‡] Feng Zuo,[§] Lixia Rong,[§] Benjamin S. Hsiao,[§] and Geoffrey W. Coates[∥]

[†]*Mitsubishi Chemical Center for Advanced Materials and the Departments of Materials and Chemical Engineering, University of California, Santa Barbara, California 93106,* [‡]*Mitsubishi Science and Technology Research Center 1000, Kamoshida-cho, Aoba-ku, Yokohama 227-8502, Japan,* [§]*Department of Chemistry, Stony Brook University, Stony Brook, New York 11974-3400,* [∥]*Department of Chemistry and Chemical Biology, Baker Laboratory Cornell University, Ithaca, New York 14853, and* [⊥]*CAS Key Laboratory of Engineering Plastics, Beijing National Laboratory for Molecular Sciences, Institute of Chemistry, Chinese Academy of Sciences, Beijing, 100190 P. R. China.* [#] *Present address: CAS Key Laboratory of Soft Matter Chemistry, Department of Polymer Science and Engineering, University of Science and Technology of China, Hefei, Anhui Province 230026, P. R. China*

Received May 27, 2010; Revised Manuscript Received July 5, 2010

ABSTRACT: Gels of syndiotactic polypropylene-*b*-ethylene-propylene-rubber-*b*-syndiotactic polypropylene (sPP-EPR-sPP) were prepared by dissolving ~6 wt % of the triblock copolymer in mineral oil at 170 °C and then cooling to room temperature in several steps to crystallize the sPP block. The gel was subjected to step-cycle processing by first extending it to a given maximum tensile strain, followed by decreasing the load to zero. The cycle was then repeated to a higher maximum strain and so on until the sample either failed or it reached an ultimate predetermined strain. The true stress and true strain ε_H during each cycle were recorded, including the true strain at zero load $\varepsilon_{H,p}$ after each cycle that resulted from the plastic deformation of the sPP crystals in the gel. The initial Young's modulus E_{init} and maximum tangent modulus E_{max} in each cycle undergo dramatic changes as a function of $\varepsilon_{H,p}$, with E_{init} decreasing for $\varepsilon_{H,p} \leq 0.1$ and then increasing slowly as $\varepsilon_{H,p}$ increases to 1 while E_{max} increases rapidly over the entire range of $\varepsilon_{H,p}$, resulting in a ratio of $E_{max}/E_{init} > 1000$ at the highest maximum (nominal) strain of 20. On the basis of small-angle X-ray scattering patterns from the deformed and relaxed gels, as well as on previous results on deformation of semicrystalline random copolymers by Strobl and co-workers, we propose that the initial decrease in E_{init} with $\varepsilon_{H,p}$ is due to a breakup of the network of the original sPP crystal lamellae while the increase in E_{max} with $\varepsilon_{H,p}$ is caused by the conversion of the sPP lamellae into fibrils of an aspect ratio that increases with further plastic deformation. The gel elastic properties can be understood as those of a short fiber composite with a highly deformable matrix. At zero stress the random copolymer midblock chains that connect the fibrils cause these to make all angles to the tensile axis (low E_{init}) while at the maximum strain the stiff crystalline sPP fibrils align with the tensile axis producing a strong, relatively stiff gel.

Introduction

Polymer gels have many applications, ranging from foodstuffs[1,2] to supporting frameworks for cell growth[3,4] to dielectric elastomers.[5] Normally soft polymer gels, those with a low polymer volume fraction, are rather brittle and cannot support large strains in either tension or compression. Recent pioneering experiments by Gong and co-workers at Hokkaido University have shown that soft but strong gels can be prepared that have an interpenetrating network, a so-called double network.[6,7] These networks are constructed with a tightly cross-linked primary network interpenetrated by a very loosely cross-linked secondary network. Frank and co-workers obtained similar results with double network gels built with different monomers.[8] A theoretical model by Brown offers an explanation for why these double network gels are so tough.[9,10] In this model microcracks in the primary network are stabilized against catastrophic growth by the loosely cross-linked strands of the second network, leading to a pronounced decrease in the elastic modulus of the gel after it has been cycled to large strains. This cyclic softening leads to a hysteretic energy loss within a thick zone of gel adjacent to the crack when a crack propagates, and thus a high fracture energy results. This softened zone has recently been detected by Gong and co-workers.[11] The cyclic softening and hysteresis in the gels are analogous to the so-called "Mullins effect" in filled elastomers,[12] although with completely different origin. In both cases the cyclic softening and hysteresis are responsible for a marked toughening of the material.

The double network approach to toughening gels, however, has the disadvantage that once the primary network has been broken it no longer contributes to the toughening. No rehealing of the network is possible unlike the case of filled elastomers, which can recover much of their hysteretic behavior over time. Double network gels are also somewhat complicated to synthesize and require rather precise tuning of the structures of both networks. Gels based on thermoplastic elastomers could offer an interesting alternative. These block copolymer based gels have been the subject of a number of recent studies in academia,[13−32] and so-called oil-extended thermoplastic elastomers have been in

*Corresponding author. E-mail: edkramer@mrl.ucsb.edu.

 Published on Web 07/28/2010

industrial use for some time. These block copolymer based gels are normally constructed from triblock copolymers with polystyrene (PS) end-blocks and polybutadiene, polyisoprene, or their hydrogenated counterparts as rubbery mid-blocks. Normally oils are chosen as swelling agents that are good solvents for the mid-blocks but nonsolvents for the PS end-blocks; a typical choice for the triblock copolymer is poly(styrene-*b*-ethylene-*r*-butene-*b*-styrene) (SEBS). Spontak and co-workers have measured the stress−strain properties of gels of various SEBS block copolymers in mineral oil up to strains of 400%.[5] They demonstrated that the Young's modulus of these gels can be tuned from less than 10 kPa to just under 200 kPa by increasing the wt % SEBS from 10 to 30%. Such gels show relatively small cyclic hysteresis or "Mullins effect" up to a tensile strain of 400%; however, the hysteretic toughening mechanism referred to above will presumably not be very important. Other mechanisms, such as plastic deformation and chain pull−out from the PS end block spheres, may be more important energy dissipating mechanisms at the crack tip.

An alternative method to produce tough gels is to replace the glassy end-blocks by semicrystalline ones.[19] In this case lamellar polymer crystals would replace the glassy spheres as network points. But unlike the glassy PS spheres of SEBS whose PS ends are unentangled, the crystals can be plastically deformed and should strain harden significantly. Indeed, a series of excellent papers by Strobl and co-workers on the plastic deformation of semicrystalline polymers and random copolymers demonstrate that the stress−strain properties of these can be understood as the breakup of a network of lamellar crystals at relatively small strains followed by a conversion of the (now separated) lamellar crystals into fibrils at larger strains.[33−41] Such a transformation, if carried out on the polymer crystals in a block copolymer gel, would result in elongated crystalline polymer fibrils in a rubbery gel matrix. At low strains these might be expected to be nearly isotropic while at larger strains they would align along the tensile direction, producing a self-aligning short fiber composite with a very soft matrix.

New polymerization methods, as well as older methods that depend on hydrogenation of anionically polymerized block copolymers with diene blocks, now make it possible to synthesize block copolymers with semicrystalline blocks suitable for testing these ideas.[42−54] In this paper we examine the mechanical properties of gels of a syndiotactic polypropylene-*b*-ethylene-*r*-propylene-*b*-syndiotactic polypropylene (sPP-EPR-sPP) triblock copolymer prepared with mineral oil. The step-cycle stress−strain curves of these gels show remarkable hysteresis and strain hardening due to the deformation of the crystals, and small-angle X-ray scattering provides evidence of the alignment of polymer fibrils at the highest strains.

Experimental Section

Materials and Gel Preparation. A triblock copolymer of syndiotactic polypropylene-*b*-ethylene-propylene-rubber-*b*-syndiotactic polypropylene (sPP-EPR-sPP) was prepared as described previously.[42,46] It had a total number-average molecular mass, M_n, of 298 kg/mol, polydispersity, $M_w/M_n = 1.20$, and the sPP blocks of nearly equal molecular mass comprising 24 wt % of the total copolymer. The ethylene mole fraction in the rubbery mid-block was 0.66. The crystallinity X_c by differential scanning calorimetry of the sPP blocks in the undiluted sPP-EPR-sPP was 28.3%. The stress−strain curves of the neat triblock copolymer can be found in a previous publication.[46] Mineral oil (Fisher Chemical, Heavy (USP/FCC) 8042-47-5 paraffin, Fisher Scientific) was used with no further purification. The gel comprised of sPP-EPR-sPP and mineral oil diluent was prepared as follows: A mixture of ∼6 wt % sPP-EPR-sPP powder in mineral oil was prepared in a vial. The mixture was heated in a vacuum oven to 170 °C for 15 h, then annealed sequentially, and held at the following temperatures—150 °C for 3 h, 120 °C for 2 h, and 100 °C for 27 h—followed by slow cooling in the oven to room temperature. After this treatment the mixture became a clear and transparent gel. The gel sample was then taken from the vial and recast in a Petri dish in the vacuum oven by following the same procedure described above.

Cyclic Mechanical Processing and Mechanical Testing. The gel film was cut into rectangular specimens with a thickness of about 0.5 mm, length of 7.3 mm, and width of 2.0 mm for the cyclic mechanical processing and mechanical property tests. The mechanical processing and testing were carried out using an Instron (Norwood, MA) 1123 tensile deformation test machine. The mechanical processing was performed as follows: Tensile cyclic processing was conducted stepwise at room temperature (20 °C) to progressively higher tensile strains. In each step, once the sample reached the appropriate tensile strain, the crosshead direction was reversed and the sample strain was decreased at the same nominal strain rate (∼0.07 min^{-1} based on the original sample length) until zero stress was achieved. Once the stress was fully released, the crosshead was immediately reversed, and the sample was then extended again at the same constant strain rate until it reached the next targeted maximum strain. The cyclic mechanical processing was continued until in the final cycle the targeted final strain was reached. The tensile cyclic tests were repeated on samples that had been previously cyclically processed to examine the effect of cyclic processing on the mechanical properties.

Thermogravimetric Analysis (TGA). The thermograms of the gel, mineral oil, and the triblock polymer were determined by thermogravimetric analysis (TGA). Experiments and data analysis were performed on a Mettler Toledo TGA/SDTA 851e instrument. A heating rate of 10 °C/min was selected, and the heating scan range was from 25 to 600 °C. Samples with weight of about 3 mg for the triblock copolymer and about 10 mg for the gel sample and mineral oil were used. The mass of the mineral oil was completely removed by 400 °C while the neat sPP-EPR-sPP block copolymer lost negligible mass at that temperature. The gel showed a two-step mass loss, mineral oil below 400 °C, and block copolymer above that temperature, so the TGA curve allowed a measurement of the block copolymer content of the gel.

Differential Scanning Calorimetry (DSC). DSC heating scans of both the unstretched and recovered stretched gel samples were performed at a heating rate of 10 °C/min on a DSC of model 2920 from TA Instruments, Newcastle, DE. The mass crystallinity in the gel was derived from the heat of fusion ratio $\Delta H/\Delta H_{sPP}$, considering the heat of fusion ΔH_{sPP} of 100% crystalline sPP to be 200 J/g.[55]

Optical Microscopy. The morphology of the cast sPP-EPR-sPP/mineral oil gel film with a thickness of about 0.5 mm was observed at room temperature by using a reflective Olympus polarized optical microscope under unpolarized and polarized light.

Small-Angle X-ray Scattering (SAXS) and Wide-Angle X-ray Diffraction (WAXD). Both SAXS and WAXD were carried out at the X27C beamline in the National Synchrotron Light Source (NSLS), Brookhaven National Laboratory (BNL). A three-pinhole collimator system was used to reduce the beam diameter to 0.2 mm. The wavelength of the X-ray beam was 1.371 Å. A modified Instron 4410 stretching apparatus was adapted to the three-pinhole collimated X-ray facility to perform the *in situ* SAXS study. The modification of the Instron instrument allowed the sample to be stretched symmetrically, which assured that the focused X-ray beam always illuminated the same position on the sample during deformation. The SAXS experimental procedure was as follows. The samples were cyclically processed as described above, and the time-resolved two-dimensional SAXS images were collected with a data acquisition time of 60 s per image using a MAR CCD X-ray detector (MAR

Figure 1. Photo of the sPP-EPR-sPP/mineral oil gel.

USA). The sample-to-detector distance was 1730 mm. All SAXS images were corrected for the main beam intensity fluctuations and sample absorption. The angular position of the SAXS patterns was calibrated using a silver behenate standard. For WAXD measurements, the unstretched and recovered stretched sPP-EPR-sPP/mineral oil gels were examined. Two-dimensional WAXD images were accumulated for a period of 120 s per image using a MAR CCD X-ray detector (MAR USA). The sample-to-detector distance was 122 mm. The diffraction angle was calibrated by using a polypropylene standard and an Al_2O_3 standard from the National Institute of Standards and Technology (NIST).

Results and Discussion

Thermogravimetric analysis of the sPP-EPR-sPP/mineral oil gel was used to determine the block copolymer content of the gel. In the gels described in this paper the sPP-EPR-sPP content was 6 wt %. Figure 1 shows a film of this gel in a Petri dish. It is optically clear and when touched it does not exude mineral oil.

The melting temperature and crystallinity of the sPP in the gel were measured by DSC. Before deformation the peak of the melting endotherm was at 105 °C, significantly lower than the value 134 °C of the neat block copolymer,[46] and the enthalpy of melting was 2.8 J/g, which corresponds to a crystallinity of the gel of 1.4% based on an enthalpy of melting of perfect sPP crystals of 200 J/g.[55] After deforming the gel in tension to a strain of about 36 (see Figure 3d for details) and decreasing the stress to zero, the endotherm was broadened significantly (see Supporting Information); the peak of the melting endotherm increased to 109 °C, and the enthalpy of melting was 3.4 J/g, a crystallinity of 1.7%, slightly increased from the value before deformation. Wide-angle X-ray diffraction patterns from samples subjected to large strains show very weak (200) and (020) reflections from helical form I sPP crystals as well as a stronger (110) reflection from transplanar form III crystals on a much larger amorphous halo background from the mineral oil and the rubbery mid-block (see Supporting Information).

Figures 2a and 2b are unpolarized and polarized optical micrographs, respectively, of the gel surface taken in reflection. The unpolarized optical micrograph shows a featureless surface (apart from some dust on the right side of the image). The micrograph taken using crossed polarizers shows considerable structure with what appear to be spherulites (see arrow on Figure 2b) as well as less organized crystals that we presume to be lamellae in form.

Figure 3a shows the tensile nominal stress−nominal strain curve of the gel during monotonic tensile deformation. Figure 3b shows the nominal stress−nominal strain curves during cyclic tensile deformation of the 6% sPP-EPR-sPP gel with maximum strain values increased sequentially from 0.1, 0.5, 1, 2, 3, and so on up to 17. To a reasonable approximation, the monotonic nominal stress−nominal strain curve of Figure 3a is the upper envelope of the cyclic nominal stress−nominal strain curves shown in Figure 3b. Note, however, the large hysteresis in each cycle of the curves shown in Figure 3b. In given cycle the ascending curve is quite different from that of the cycle preceding it but similar, though not identical, to the descending curve of the previous cycle. In highly crystalline polymers such curves would result from plastic deformation giving rise to progressively larger residual strain at zero stress. In the case of these gels there is little residual strain at zero stress. Instead, the curves appear very similar to those of a step-cycle test of a filled elastomer; i.e., they appear to show what in the filled elastomer literature is referred to as the "Mullins effect".[12] Figure 3c shows nominal stress−nominal strain curves for a second cyclic tensile deformation series on the same sample shown in Figure 3b after the first cyclic deformation with maximum strains of 0.1, 0.5, 1, 2, 3, and so on up to 12. For this series the strain (and sample area) is based on the dimensions of the sample at the beginning of the series; i.e., after the cyclic deformation of Figure 3b the sample length and area were remeasured. Note that at high maximum strains the nominal stresses σ_n in each cycle are somewhat larger than those of the corresponding cycle in Figure 3b; this is largely because the sample area at the start of the second series has decreased due to some plastic deformation. But note also that the shape of the ascending curves is now concave-upward, the hysteresis in each cycle is decreased, and the envelope of these curves is very different from the monotonic nominal stress−nominal strain curve of Figure 3a. To emphasize this difference, we show in Figure 3d a monotonic nominal stress−nominal strain curve for a sample subjected to a step-cycle tensile process similar to that shown in Figure 3b. It is clear that this nominal stress−nominal strain curve is very different from the monotonic nominal stress−nominal strain curve of the gel as prepared (Figure 3a). The very small initial slope corresponds to a very soft material with a very low elastic modulus, whereas the maximum tangent modulus and maximum stress are quite high. If we convert the maximum nominal stress to a maximum true stress and then correct for the fact that the gel has only 6 wt % block copolymer, the maximum true stress on the polymer strands in the gel network is 600 MPa, a very respectrable value for a steel![56] Even then, the gel slipped from the grips, instead of breaking somewhere in the highly stretched midsection of the sample. Clearly these semicrystalline block copolymer gels are very strong and tough.

The elastic recovery at zero stress after the maximum strain ε_{max}, defined as $100 \times (\varepsilon_{max} - \varepsilon(0,\varepsilon_{max}))/\varepsilon_{max}$, where ε_{max} and $\varepsilon(0,\varepsilon_{max})$ are the maximum strain and the strain in the cycle at zero stress after the maximum strain ε_{max}, respectively, is shown in Figure 3e. Elastic recovery reported in this way is a normal way of assessing the elastic performance of an elastomer but is slightly misleading for materials with such large nominal strains to failure as these gels. The reasons for the excellent elastic recovery of these gels will be considered after data on similar samples have been analyzed using an approach suggested by Strobl and coworkers.[33−41]

It has long been realized that for highly deformable materials extension ratios L/L_0 or true (or Hencky) strains $\varepsilon_H \equiv \ln(L/L_0)$ should be used to properly analyze data. Therefore, following Strobl and co-workers, we determine both the true stress $\sigma_t = \sigma_n L/L_0$ and ε_H during each cycle. We then represent the maximum true strain in each cycle as the sum of an elastic component $\varepsilon_{H,e}$ and a plastic component $\varepsilon_{H,p}$ where the latter is determined from the length of the sample after the stress has been decreased to zero. In Figure 4, we plot the elastic and plastic true strains versus the total true strain at the maximum of each cycle.

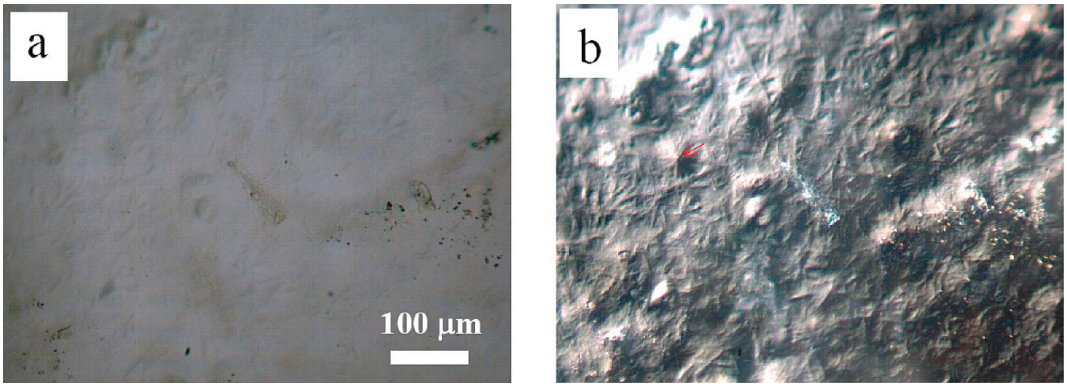

Figure 2. Reflection optical micrographs of the unstretched 6% sPP-EPR-sPP/mineral oil gel film under (a) unpolarized light and (b) polarized light with crossed polarizer and analyzer. The magnification of (b) is the same as (a).

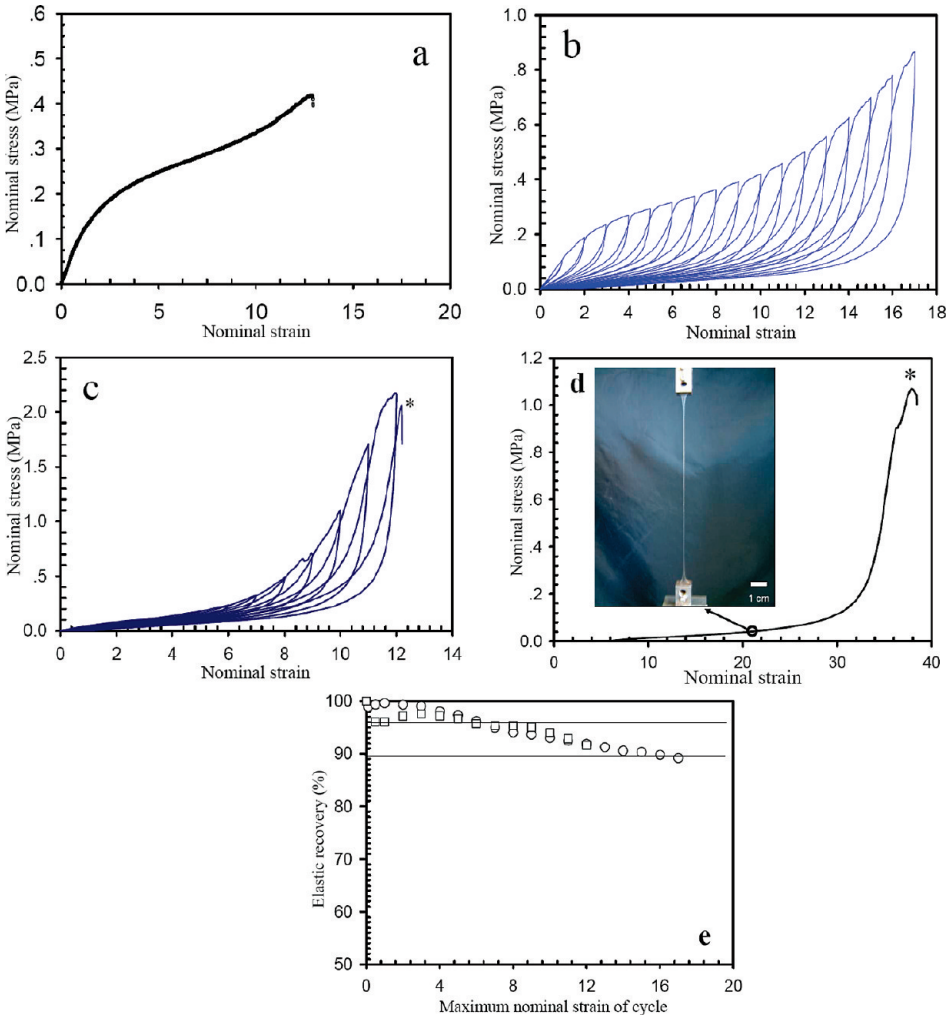

Figure 3. Nominal stress−nominal strain curves of the 6% sPP-EPR-sPP/mineral oil gel during (a) monotonic tensile deformation; (b) cyclic tensile deformation with maximum strains of 0.1, 0.5, 1, 2, 3, and so on up to 17; (c) after the first cyclic deformation series a second cyclic tensile deformation series on the same sample with maximum strains of 0.1, 0.5, 1, 2, 3, and so on up to 12. An asterisk indicates the specimen slipped from one of the grips. For this series the strain (and sample area) is calculated based on the dimensions of the sample at the beginning of the series. (d) Monotonic nominal stress−nominal strain curve of a 6% sPP-EPR-sPP/mineral oil gel after an initial cyclic tensile deformation procedure similar to that shown in (b). Note that the stress and strain are based on the original sample dimensions, before the initial cyclic tensile deformation. The photo in the inset was taken at a strain of 21 marked by the circle. The scale bar is 1 cm. (e) Elastic recovery as a function of the maximum strain during the two cyclic mechanical processing series shown in (b) (squares) and (c) (circles).

The plastic true strain is low up to a true strain of 2 but then grows rapidly as the maximum true strain in each cycle increases while above a true strain of 2 the elastic true strain saturates at a value of about 1.9 (extension ratio ~8). This behavior is qualitatively similar to, but quantitatively quite different than, that observed by Strobl et al. on semicrystalline random copolymers. The main difference is that for most of his samples point C occurs at true strains between 0.4 and 0.8. Strobl's interpretation

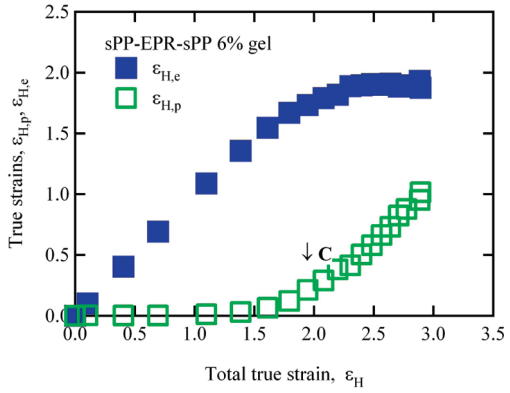

Figure 4. Plastic and elastic true strains in a 6% sPP-EPR-sPP/mineral oil gel versus the total true strain at the maximum of each cycle of a step-cycle tensile test. A true strain of 3 corresponds to an extension ratio of ~20. The arrow at C marks fibril formation according to the model of Strobl.

for his samples is that the initial "yield" seen in the nominal stress−nominal strain curve most clearly corresponds to the breaking apart of a connected network of lamellae into individual lamellae. With further deformation the individual lamellae are broken into small blocks but retain their thicknesses. Finally at the point where the elastic true strain saturates, the slope of the true plastic strain versus true strain curve increases, according to Strobl, as a result of converting the connected blocks of crystalline lamellae into long crystalline fibrils. A further increase in the plastic true strain results in better fibril alignment and the necessity to extend plastically the fibrils further in the tensile direction giving rise to strong strain hardening. Finally, a regime is reached where the chains in the fibrils begin to disentangle and the elastic true strain decreases. Despite the quantitative differences between his data and ours and the obvious differences in structure of the gels versus that of the random copolymers, Strobl's interpretation seems appropriate for our samples. At very small true strains in the as-prepared gel specimens, despite the fact that the network of lamellar crystals is very sparse, the interconnected network bears more of the load than the very soft surrounding rubbery strands of the gel. Nevertheless, the increasing load on this network begins to break it apart while the lamellae themselves remain intact. When the stress is removed, the rubbery strands of the gel pull the lamellae almost back to their original positions and the residual (plastic) true strain is very low. As the true strain is increased the lamellae begin to break into blocks, with some lamellae, because of their orientation with respect to the tensile stress, undergoing this transformation at higher true stresses and true strains than others. Still the residual strain when the stress is removed is small since the elements of the lamellae remain in close proximity. Finally, however, as the connected lamellar blocks are converted into fibrils, the residual true strain increases rapidly and the elastic true strain saturates at point C in Figure 4. At these high true strains the gel becomes like a short fiber composite with aligned fibers and a very soft (rubbery gel strand) matrix. The only way such an aligned fiber composite can be further plastically deformed along the alignment direction is to deform the fibers (in our case the crystalline fibrils).

To test this hypothesis, we conducted small-angle X-ray scattering (SAXS) experiments at various points in the step-cycle testing of the gels. Figure 5 shows both the nominal stress versus nominal strain curve and SAXS patterns at various points in a cycle with a maximum true strain of 2.4. At strains near the maximum of the cycle an intensity streak normal to the tensile axis appears due to the oriented fibrils and is clearly visible in the SAXS pattern. At the much lower stresses and strains in the cycle

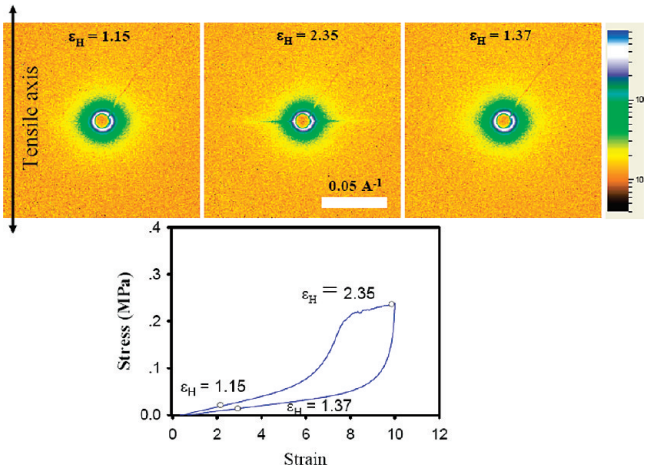

Figure 5. Small-angle X-ray scattering patterns taken during one cycle of a step-cycle tensile test. The nominal stress−nominal strain diagram shows the points (circles) and true strains at which the SAXS patterns were taken.

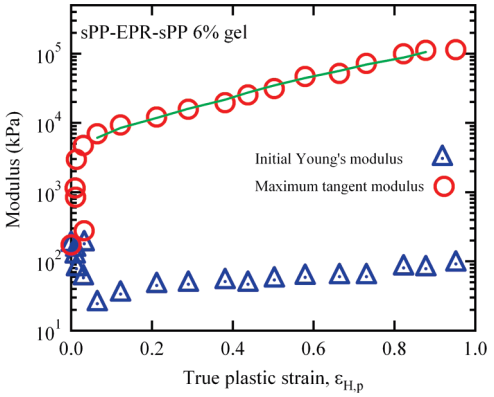

Figure 6. Initial Young's modulus and maximum tangent modulus in each step cycle as a function of the true plastic strain at the end of the previous cycle for the 6 wt % sPP-EPR-sPP/mineral oil gel. The solid line is the prediction of the short fiber composite model (see text below).

the rubbery chains in the gel have relaxed, the fibrils become disoriented and the streak disappears. A much more extensive set of X-ray experiments on similar gels from which the mineral oil has been removed show very similar SAXS streaks that develop after the point C on a "Strobl plot" like that shown in Figure 4.[57]

The effects of these morphological changes in the gel are also apparent in a plot of the initial (low strain) modulus and the maximum tangent modulus of the gel as a function of the true plastic strain at the end of the previous cycle shown in Figure 6. The moduli are computed from the slopes of the loading true stress versus total true strain curves. The initial Young's modulus first decreases from about 200 kPa to about 30 kPa during the initial step cycles while the maximum tangent modulus increases from 200 kPa to 10 MPa. These changes occur as the true plastic strain increases from 0 to about 0.1, corresponding roughly to a total true strain of 2, i.e., point C in Figure 4, where fibril formation has occurred according to the model of Strobl. For larger plastic true strains the initial Young's modulus increases modestly to about 80 kPa for a plastic true strain approaching 1 while the maximum tangent modulus increases roughly exponentially with true plastic strain until it reaches a value of over 100 MPa. If we correct this final tangent modulus for the mineral oil content of the gel which is assumed to bear no load, the maximum tangent modulus of the polymer chains in the gel is nearly 2 GPa. It is worth pointing out that in each cycle the maximum tangent

modulus occurs at a total true strain that is approximately the maximum true strain in the previous cycle. The decrease in tangent modulus past this point in the cycle is apparently due to the increased contribution of plastic strain to the total strain.

It is interesting that the maximum tangent modulus increases exponentially with plastic strain past the strain at which fibril formation occurs. It suggests that the fibrils, once formed, can be further plastically deformed, becoming longer and thinner. In each cycle just before this plastic deformation of the fibers occurs, the modulus of the gel should be that of a short fiber composite, whose modulus will depend on the aspect ratio (= length/radius) of the fibers, the area fraction of fibers, the shear modulus of the soft matrix, and the Young's modulus of the fibers. To show that this is a reasonable picture for the mechanical properties of the fibrillar gel, we use a model of such a fiber composite first proposed by Odell and Keller[58] based on the shear lag model of Cox.[59] In this approach the Young's modulus E_c of the composite is given by

$$E_c = E_f V_f \left[1 - \frac{\tanh(\beta l/2)}{\beta l/2}\right] + E_m(1 - V_f) \quad (1)$$

where V_f is the area fraction of the fibers, E_f is the Young's modulus of the fibers, E_m is the Young's modulus of the matrix, l is the length of the fibers, and β is given by

$$\beta = \frac{1}{r}\sqrt{\frac{2G_m}{E_f((R/r) - 1)}} \quad (2)$$

where G_m is the shear modulus of the matrix, r is the radius of the fibrils, and $(R/r)^2 = 1/V_f$. In our case the fibrils are assumed to deform plastically at constant volume so that $l = l_C \exp(\varepsilon_{H,p,C})$ and $r = r_C/\exp(\varepsilon_{H,p,C}/2)$, where $\varepsilon_{H,p,C}$ is the plastic true strain after point C in Figure 4 and l_C and r_C are the fibril lengths and radii at point C. Finally, we estimate that the area fraction of fibrils $V_f = (V_f)_0 \exp(\varepsilon_H)/\exp(\varepsilon_{H,p})$; this assumes that all the elastic deformation is in the matrix and all the plastic deformation occurs in the fibrils. Choosing values of r_C and l_C of 6 and 200 nm, values that are consistent with the SAXS streak normal to the tensile axis, and realizing that if $E_f > 10$ GPa, the values of E_c are insensitive to the choice of E_f, we are left with one free parameter G_m since for a rubbery matrix $E_m \approx 3G_m$. Adjusting this parameter to obtain the best fit to the data results in the solid curve shown in Figure 6 for a G_m value of 350 kPa. Realizing that G_m is not the initial modulus of the gel but the shear modulus after an elastic extension ratio ($\exp(\varepsilon_{H,e})$) greater than 4, this value seems reasonable.

The results of these step-cycle experiments on the sPP-EPR-sPP gels may be related to interesting recent results on neat poly(propylene) copolymers with 12 mol % ethylene of Hiltner and co-workers.[60] They observed large hysteretic changes in the tensile nominal stress−nominal strain curves that are qualitatively similar to both those observed by us here and also those observed by Strobl and co-workers on homopolymers and random copolymers. However, their polypropylene crystals are isotactic, not syndiotactic, based on their WAXD patterns, and their observed decreases in initial modulus and increases in maximum tangent modulus are smaller than what we see for our gels. Hiltner and co-workers' interpretation of these changes is qualitatively similar to ours (and Strobl's) with a major difference being that they propose that a recrystallization process occurs once fibrillar structures are formed producing shish-kabob structures. They observe SAXS patterns with intense diffraction peaks along the tensile axis, which they attribute to lamellar overgrowths on the fibrils, as well as a fibril scattering streak normal to the tensile axis. In our drawn block copolymer gels we observe only the scattering streak from the fibrils. Hiltner and co-workers observed quite different results for a PP copolymer with a larger content of ethylene (17%).[61] The initial monotonic nominal stress−strain curve showed soft elastomeric properties and modest strain hardening. Subsequent tensile stress−strain curves showed a much larger initial Young's modulus (24 MPa vs 6 MPa) and nearly linear strain hardening—the initial tensile strain produced a much stiffer material. These results were attributed to the formation of a second lamellar network of daughter α PP crystal lamellae on the PP oriented fibrils. Clearly our sPP-EPR-sPP gels behave quite differently.

Finally, it is appropriate to discuss why these gels are so tough. As pointed out in the Introduction, hysteresis losses during crack propagation are very important in dictating the toughness of elastomers and gels, and it is clear from the step-cycle tests that these gels have very significant hysteresis losses. Comparing our semicrystalline block copolymer gels with normal cross-linked (single network) gels that do not have this source of hysteresis, it is obvious that the semcrystalline gels will have superior toughness. In addition, the formation and orientation of crystalline fibrils along the tensile axis provide a sources of toughness usually associated with unidirectional fiber composites. Even if a given fibril fails, the surrounding fibrils are strong enough to bear the additional load and prevent the resulting nanometer scale crack that forms from propagating catastrophically.

Conclusions

Gels of semicrystalline sPP-EPR-sPP triblock copolymers have remarkable mechanical properties after step-cycle mechanical processing that combine softness at small deformations with high stiffness and strength at large extension. They have very low initial Young's moduli but very high tangent moduli at larger strains that on a true stress−true strain basis can be more than 3 orders of magnitude larger than the soft initial moduli. In addition, these physical gels, unlike dilute chemically cross-linked single network gels, are exceptionally tough and have very large strains to break. The key to these excellent properties apparently is the fact that the crystalline lamellae in the original gel can be plastically transformed into fibrils by the step-cycle processing and can be further plastically deformed to crystalline fibrils with larger and larger aspect ratios by the increasing maximum strain of the step-cycle process. A model of the uniaxially deformed gel as a short fiber composite can capture the increase in the maximum tangent modulus with plastic strain using reasonable values for the geometry and elastic properties of the sPP crystal fibers and the rubbery gel matrix.

Acknowledgment. We appreciate the financial support of the Mitsubishi Chemical Center for Advanced Materials at UCSB. We made use of the UCSB MRL Central Facilities funded through the NSF MRSEC Program (DMR 0520415) and the Cornell Center for Materials Research Shared Experimental Facilities funded through the NSF MRSEC Program (DMR 0520404). Use of the National Synchrotron Light Source, Brookhaven National Laboratory, was supported by the U.S. Department of Energy, Office of Science, Office of Basic Energy Sciences, under Contract DE-AC02-98CH10886.

Supporting Information Available: DSC heating scan curves, a WAXD pattern, and calculation of fibril diameter and length. This material is available free of charge via the Internet at http://pubs.acs.org.

References and Notes

(1) Donald, A. M. *Nature Mater.* **2004**, *3*, 579–581.
(2) Donald, A. M. *J. Polym. Sci., Polym. Phys.* **2007**, *45*, 3257–3262.
(3) Little, L.; Healy, K. E.; Schaffer, D. V. *Chem. Rev.* **2008**, *108*, 1787–1796.

(4) Saha, K.; Irwin, E. F.; Kozhukh, J.; Schaffer, D. V.; Healy, K. E. *J. Biomed. Mater. Res., Part A* **2007**, *81A*, 240–249.
(5) Shankar, R.; Krishnan, A. K.; Ghosh, T. K.; Spontak, R. J. *Macromolecules* **2008**, *41*, 6100–6109.
(6) Na, Y. H.; Kurokawa, T.; Katsuyama, Y.; Tsukeshiba, H.; Gong, J. P.; Osada, Y.; Okabe, S.; Karino, T.; Shibayama, M. *Macromolecules* **2004**, *37*, 5370–5374.
(7) Tanaka, Y.; Kuwabara, R.; Na, Y.-H.; Kurokawa, T.; Gong, J. P.; Osada, Y. *J. Phys. Chem. B* **2005**, *109*, 11559–11562.
(8) Myung, D.; Waters, D.; Wiseman, M.; Duhamel, P.-E.; Noolandi, J.; Ta, C. N.; Frank, C. W. *Polym. Adv. Technol.* **2008**, *19*, 647–657.
(9) Brown, H. R. *Macromolecules* **2007**, *40*, 3815–3818.
(10) Webber, R. E.; Creton, C.; Brown, H. R.; Gong, J. P. *Macromolecules* **2007**, *40*, 2919–2927.
(11) Yu, Q. M.; Tanaka, Y.; Furukawa, H.; Kurokawa, T.; Gong, J. P. *Macromolecules* **2009**, *42*, 3852–3855.
(12) Mullins, L. *Rubber Chem. Technol.* **1969**, *42*, 339–361.
(13) Mortensen, K.; Brown, W.; Norden, B. *Phys. Rev. Lett.* **1992**, *68*, 2340–2343.
(14) Mortensen, K.; Pedersen, J. S. *Macromolecules* **1993**, *26*, 805–812.
(15) Laurer, J. H.; Bukovnik, R.; Spontak, R. J. *Macromolecules* **1996**, *29*, 5760–5762.
(16) Quintana, J. R.; Diaz, E.; Katime, I. *Macromol. Chem. Phys.* **1996**, *197*, 3017–3026.
(17) Kleppinger, R.; Mischenko, N.; Theunissen, E.; Reynaers, H. L.; Koch, M. H. J.; Almdal, K.; Mortensen, K. *Macromolecules* **1997**, *30*, 7012–7014.
(18) Laurer, J. H.; Mulling, J. F.; Khan, S. A.; Spontak, R. J.; Bukovnik, R. *J. Polym. Sci., Polym. Phys.* **1998**, *36*, 2379–2391.
(19) Kleppinger, R.; van Es, M.; Mischenko, N.; Koch, M. H. J.; Reynaers, H. L. *Macromolecules* **1998**, *31*, 5805–5809.
(20) Laurer, J. H.; Mulling, J. F.; Khan, S. A.; Spontak, R. J.; Lin, J. S.; Bukovnik, R. *J. Polym. Sci., Polym. Phys.* **1998**, *36*, 2513–2523.
(21) Kleppinger, R.; Mischenko, N.; Reynaers, H.; Koch, M. H. J. *J. Polym. Sci., Part B: Polym. Phys.* **1999**, *37*, 1833–1840.
(22) Laurer, J. H.; Khan, S. A.; Spontak, R. J.; Satkowski, M. M.; Grothaus, J. T.; Smith, S. D.; Lin, J. S. *Langmuir* **1999**, *15*, 7947–7955.
(23) Spontak, R. J.; Wilder, E. A.; Smith, S. D. *Langmuir* **2001**, *17*, 2294–2297.
(24) Quintana, J. R.; Hernáez, E.; Katime, I. *J. Phys. Chem. B* **2001**, *105*, 2966–2970.
(25) Vega, D. A.; Sebastian, J. M.; Loo, Y. L.; Register, R. A. *J. Polym. Sci., Polym. Phys.* **2001**, *39*, 2183–2197.
(26) Walker, T. A.; Semler, J. J.; Leonard, D. N.; van Maanen, G. J.; Bukovnik, R. R.; Spontak, R. J. *Langmuir* **2002**, *18*, 8266–8270.
(27) Quintana, J. R.; Hernáez, E.; Katime, I. *Polymer* **2002**, *43*, 3217–3222.
(28) Inomata, K.; Nakanishi, D.; Banno, A.; Nakanishi, E.; Abe, Y.; Kurihara, R.; Fujimoto, K.; Nose, T. *Polymer* **2003**, *44*, 5303–5310.
(29) Drzal, P. L.; Shull, K. R. *Macromolecules* **2003**, *36*, 2000–2008.
(30) Drzal, P. L.; Shull, K. R. *Eur. Phys. J. E* **2005**, *17*, 477–483.
(31) Seitz, M. E.; Burghardt, W. R.; Faber, K. T.; Shull, K. R. *Macromolecules* **2007**, *40*, 1218–1226.
(32) Seitz, M. E.; Martina, D.; Baumberger, T.; Krishnan, V. R.; Hui, C.-Y.; Shull, K. R. *Soft Matter* **2009**, *5*, 447–456.
(33) Hiss, R.; Hobeika, S.; Lynn, C.; Strobl, G. *Macromolecules* **1999**, *32*, 4390–4403.
(34) Hobeika, S.; Men, Y.; Strobl, G. *Macromolecules* **2000**, *33*, 1827–1833.
(35) Men, Y.; Strobl, G. *J. Macromol. Sci., Part B: Phys.* **2001**, *40*, 775–796.
(36) Al-Hussein, M.; Strobl, G. *Macromolecules* **2002**, *35*, 8515–8520.
(37) Men, Y.; Rieger, J.; Strobl, G. *Phys. Rev. Lett.* **2003**, *91*, 0905502.
(38) Men, Y.; Strobl, G. *Macromolecules* **2003**, *36*, 1889–1898.
(39) Hong, K.; Rastogi, A.; Strobl, G. *Macromolecules* **2004**, *37*, 10165–10173.
(40) Hong, K.; Rastogi, A.; Strobl, G. *Macromolecules* **2004**, *37*, 10174–10179.
(41) Hong, K.; Strobl, G. *Macromolecules* **2006**, *39*, 268–273.
(42) Tian, J.; Husted, P. D.; Coates, G. W. *J. Am. Chem. Soc.* **2001**, *123*, 5134–5135.
(43) Cherian, A. E.; Rose, J. M.; Lobkovsky, E. B.; Coates, G. W. *J. Am. Chem. Soc.* **2005**, *127*, 13770–13771.
(44) Harney, M. B.; Zhang, Y. H.; Sita, L. R. *Angew. Chem., Int. Ed.* **2006**, *45*, 2400–2404.
(45) Arriola, D. J.; Carnahan, E. M.; Hustad, P. D.; Kuhlman, R. L.; Wenzel, T. T. *Science* **2006**, *312*, 714–719.
(46) Hotta, A.; Cochran, E. W.; Ruokolainen, J.; Khanna, V.; Fredrickson, G. H.; Kramer, E. J.; Shin, Y. W.; Shimizu, F.; Cherian, A. E.; Hustad, P. D.; Rose, J. M.; Coates, G. W. *Proc. Natl. Acad. Sci. U.S.A.* **2006**, *103*, 15327–15332.
(47) Diamanti, S. J.; Khanna, V.; Hotta, A.; Coffin, R. C.; Yamakawa, D.; Kramer, E. J.; Fredrickson, G. H.; Bazan, G. C. *Macromolecules* **2006**, *39*, 3270–3274.
(48) Hustad, P. D.; Kuhlman, R. L.; Arriola, D. J.; Carnahan, E. M.; Wenzel, T. T. *Macromolecules* **2007**, *40*, 7061–7064.
(49) Coffin, R. C.; Diamanti, S. J.; Hotta, A.; Khanna, V.; Kramer, E. J.; Fredrickson, G. H.; Bazan, G. C. *Chem. Commun.* **2007**, 3550−3552 (DOI: 10.1039/b705808j).
(50) Edson, J. B.; Wang, Z.; Kramer, E. J.; Coates, G. W. *J. Am. Chem. Soc.* **2008**, *130*, 4968–4977.
(51) Rose, J. M.; Deplace, F.; Lynd, N. A.; Wang, Z.; Hotta, A.; Lobkovsky, E. B.; Kramer, E. J.; Coates, G. W. *Macromolecules* **2008**, *41*, 9548–9555.
(52) Koo, C. M.; Wu, L. F.; Lim, L. S.; Mahanthappa, M. K.; Hillmyer, M. A.; Bates, F. S. *Macromolecules* **2005**, *38*, 6090–6098.
(53) Koo, C. M.; Hillmyer, M. A.; Bates, F. S. *Macromolecules* **2006**, *39*, 667–677.
(54) Myers, S. B.; Register, R. A. *Macromolecules* **2009**, *42*, 6665–6670.
(55) Haftka, S.; Könnecke, K. *J. Macromol. Sci., Part B: Phys.* **1991**, *30*, 319–334.
(56) Pickering, F. B. Structure-Property Relationships in Steel. In *Materials Science and Technology−A Comprehensive Treatment*; Cahn, R. W., Haasen, P., Kramer, E. J., Eds.; VCH: Weinheim, 1992; Vol. *7*, Chapter 2, p 41.
(57) Deplace, F.; Wang, Z.; Lynd, N. A.; Hotta, A.; Rose, J. M.; Hustad, P.; Tian, J.; Ohtaki, H.; Coates, G. W.; Shimizu, F.; Hirokane, K.; Yamada, F.; Shin, Y.-W.; Rong, L.; Toki, S.; Hsiao, B. S.; Fredrickson, G. H.; Kramer, E. J. *J. Polym. Sci., Polym. Phys.* **2010**, *48*, 1428–1437.
(58) Odell, J. A.; Keller, A. *Polym. Sci. Eng.* **1977**, *17*, 544–559.
(59) Cox, H. L. *Br. J. Appl. Phys.* **1952**, *3*, 72–79.
(60) Poon, B. C.; Dias, P.; Ansems, P.; Chum, S. P.; Hiltner, A.; Baer, E. *J. Appl. Polym. Sci.* **2007**, *104*, 489–499.
(61) Dias, P.; Kazmierczak, T.; Chang, A.; Ansems, P.; Van Dun, J.; Hiltner, A.; Baer, E. *J. Appl. Polym. Sci.* **2009**, *112*, 3736–3747.